Monthly Notices of the ROYAL ASTRONOMICAL SOCIETY LETTERS

Mon. Not. R. Astron. Soc. **410,** L13–L17 (2011) doi:10.1111/j.1745-3933.2010.00969.x

The Subaru Lyα blob survey: a sample of 100-kpc Lyα blobs at $z = 3^{\star}$

Y. Matsuda,[1]† T. Yamada,[2] T. Hayashino,[3] R. Yamauchi,[3] Y. Nakamura,[2,3] N. Morimoto,[2] M. Ouchi,[4,5]‡ Y. Ono,[6] K. Kousai,[3] E. Nakamura,[3] M. Horie,[3] T. Fujii,[3] M. Umemura[7] and M. Mori[7]

[1]*Department of Physics, Science Site, Durham University, South Road, Durham DH1 3LE*
[2]*Astronomical Institute, Graduate School of Science, Tohoku University, Aramaki, Aoba-ku, Sendai 980-8578, Japan*
[3]*Research Center for Neutrino Science, Graduate School of Science, Tohoku University, Sendai 980-8578, Japan*
[4]*Observatories of the Carnegie Institution of Washington, 813 Santa Barbara Street, Pasadena, CA 91101, USA*
[5]*Institute for Cosmic Ray Research, University of Tokyo, Kashiwa 277-8582, Japan*
[6]*Department of Astronomy, Graduate School of Science, The University of Tokyo, Tokyo 113-0033, Japan*
[7]*Center for Computational Sciences, University of Tsukuba, Tsukuba 305-8577, Japan*

Accepted 2010 October 13. Received 2010 October 12; in original form 2010 July 23

ABSTRACT

We present results of a survey for giant Lyα blobs (LABs) at $z = 3$ with Subaru/Suprime-Cam. We obtained Lyα imaging at $z = 3.09 \pm 0.03$ around the SSA22 protocluster and in several blank fields. The total survey area is 2.1 deg^2, corresponding to a comoving volume of 1.6×10^6 Mpc^3. Using a uniform detection threshold of 1.4×10^{-18} erg s^{-1} cm^{-2} arcsec^{-2} for the Lyα images, we construct a sample of 14 LAB candidates with major-axis diameters larger than 100 kpc, including five previously known blobs and two known quasars. This survey triples the number of known LABs over 100 kpc. The giant LAB sample shows a possible 'morphology–density relation': filamentary LABs reside in average density environments as derived from compact Lyα emitters, while circular LABs reside in both average density and overdense environments. Although it is hard to examine the formation mechanisms of LABs only from the Lyα morphologies, more filamentary LABs may relate to cold gas accretion from the surrounding intergalactic medium (IGM) and more circular LABs may relate to large-scale gas outflows, which are driven by intense starbursts and/or by active galactic nucleus activities. Our survey highlights the potential usefulness of giant LABs to investigate the interactions between galaxies and the surrounding IGM from the field to overdense environments at high redshift.

Key words: galaxies: evolution – galaxies: formation – galaxies: high-redshift – cosmology: observations – early Universe.

1 INTRODUCTION

Lyα blobs (LABs) are spatially extended Lyα nebulae seen in the high-redshift Universe (e.g. Francis et al. 1996; Keel et al. 1999; Steidel et al. 2000; Matsuda et al. 2004; Palunas et al. 2004; Dey et al. 2005; Nilsson et al. 2006; Greve et al. 2007; Smith & Jarvis 2007; Saito et al. 2006, 2008; Prescott, Day & Jannuzi 2009; Ouchi et al. 2009; Yang et al. 2009, 2010). LABs are thought to relate to the formation of massive galaxies (Dey et al. 2005; Matsuda et al. 2006) and to be indicative of strong interactions between the intergalactic medium (IGM) and galaxies with intense star formation activities and/or active galactic nuclei (AGNs) (Furlanetto et al. 2005). To explain the formation mechanisms of LABs, at least three possible ideas have been proposed: cold gas accretion, galactic winds and photoionization by central galaxies or by AGNs (Haiman, Spaans & Quataert 2000; Taniguchi & Shioya 2000; Chapman et al. 2001). In spite of extensive observational and theoretical efforts in the decade after the first discovery of LABs, the formation mechanisms of LABs are still controversial (Mori & Umemura 2006; Dijkstra & Loeb 2009; Geach et al. 2009; Scarlata et al. 2009; Faucher-Giguere et al. 2010; Goerdt et al. 2010; Shimizu & Umemura 2010).

Among the LABs, special attention has been given to the largest examples with the spatial extents of ∼100–200 kpc (hereinafter giant LABs) because of their spectacular morphologies and possible association with protoclusters (Steidel et al. 2000; Palunas et al. 2004; Prescott et al. 2008; Matsuda et al. 2009). At present, there are only six known giant LABs over 100 kpc and they have been

⋆Based on data collected at the Subaru Telescope, which is operated by the National Astronomical Observatory of Japan.

†E-mail: yuichi.matsuda@durham.ac.uk
‡Carnegie Fellow.

selected by using different quality data sets and different methods (Francis et al. 1996; Steidel et al. 2000; Dey et al. 2005; Greve et al. 2007; Matsuda et al. 2009). It is therefore difficult to examine their statistical properties. In order to construct a statistically reliable sample of giant LABs and so to test their possible association with overdense environments, we undertook a deep, wide-field Lyα imaging at $z = 3.1$.

In this Letter, we use AB magnitudes and adopt cosmological parameters, $\Omega_{\rm M} = 0.3, \Omega_\Lambda = 0.7$ and $H_0 = 70$ km s^{-1} Mpc^{-1}. In this cosmology, the Universe at $z = 3.1$ is 2.0 Gyr old and 1.0 arcsec corresponds to a physical length of 7.6 kpc at $z = 3.1$.

2 OBSERVATIONS AND DATA REDUCTION

We briefly describe our observations and data reduction, although the details will be reported in a separate paper (Yamada et al., in preparation). The summary of the observations and data is listed in Table 1. The imaging observations were carried out between 2002 September and 2005 October using Suprime-Cam (Miyazaki et al. 2002) on the 8.2-m Subaru Telescope (Iye et al. 2004). Suprime-Cam has a pixel scale of 0.2 arcsec and a field of view of 34 $\times$ 27 arcmin^2. We obtained narrow-band (*NB*497) images for 12 pointings: Great Observatories Origins Deep Survey-North (GOODS-N), Subaru Deep Field (SDF), three fields in Subaru-XMM Deep Survey (SXDS-C, N, and S) and seven fields around SSA22a (SSA22-Sb1-7). The SSA22-Sb1 field was the first field of our survey and centred at SSA22a, which contains the protocluster region at $z = 3.09$ discovered by Steidel et al. (2000). Initial results of the observations in the SSA22-Sb1 field have been already published (Hayashino et al. 2004; Matsuda et al. 2004, 2005, 2006). The *NB*497 filter has a central wavelength of 4977 Å and full width at half-maximum (FWHM) of 77 Å, which corresponds to the redshift range for Lyα at $z = 3.062$–3.126 (Hayashino et al. 2004). The width of the redshift slice is 59 comoving Mpc. For the SSA22 fields, we obtained broad-band (*B* and *V*) images in our observing runs. For the GOODS-N, we used archival raw *B*- and *V*-band images (Capak et al. 2004). For the SDF and SXDS fields, we used public, reduced *B*- and *V*-band images (Kashikawa et al. 2004; Furusawa et al. 2008).

We reduced the raw data with SDFRED (Yagi et al. 2002; Ouchi et al. 2003) and IRAF. We calibrated the astrometry of the images using the 2MASS All-Sky Catalog of Point Sources (Cutri et al. 2003). For photometric calibration, we used the photometric and spectrophotometric standard stars, SA113, SA115, FEIGE34, Hz44, P177D, GD248, SA95-42, LDS749B, BD +332642 and G24-9 (Oke 1990; Landolt 1992). We corrected the magnitudes using the Galactic extinction map of Schlegel, Finkbeiner & Dacis (1998). We aligned the combined images and smoothed with Gaussian kernels to match their seeing to an FWHM of 1.0 or 1.1 arcsec, depending on the original seeing. We made *BV* images [$BV = (2B + V)/3$] for the continuum at the same effective wavelength as *NB*497 and made $NB_{\rm c}$ (continuum-subtracted *NB*497) images for emission-line images. The total survey area after masking low signal-to-noise ratio regions and bright stars is 2.12 deg^2 and the survey volume is 1.6 $\times$ 10^6 comoving Mpc^3. This is 12 times larger than the survey area of Matsuda et al. (2004) and 100 times larger than that of Steidel et al. (2000). The 1σ surface brightness limits of the $NB_{\rm c}$ images are (0.7–1.2) $\times$ 10^{-18} erg s^{-1} cm^{-2} arcsec^{-2}.

3 RESULTS

Object detection and photometry are performed using the double image mode of SExtractor version 2.5.0 (Bertin & Arnouts 1996). For source detection, we use smoothed $NB_{\rm c}$ images with Gaussian kernels to match their seeing to an FWHM of 1.4 arcsec in order to slightly increase the sensitivities for diffuse extended sources and to make all the images the same seeing size. We use the same detection threshold (DETECT-THRESH) of 1.4 $\times$ 10^{-18} erg s^{-1} cm^{-2} arcsec^{-2} (or 28.5 mag arcsec^{-2}) for all the 12 fields. The magnitudes and colours are measured with isophotal apertures defined in the $NB_{\rm c}$ images.

In Fig. 1, we plot the $BV - NB497$ colours and $NB_{\rm c}$ magnitudes of the $NB_{\rm c}$-detected sources. The solid line represents the colour criterion used for narrow-band excess objects, $BV - NB497 = 0.7$, which corresponds to an observed equivalent width of EW$_{\rm obs}$ = 80 Å. From these narrow-band excess objects, we make a diameter-limited catalogue of 14 LABs down to a major-axis diameter of the isophotal aperture of $a \geq 13$ arcsec (or $\geq$100 kpc at $z = 3.1$).

For the LAB selection, we use the major-axis diameters rather than isophotal area, in order to cover LABs with asymmetric structures. For example, cold stream models predicted that LABs have asymmetric, long and thin filaments (Faucher-Giguere et al. 2010; Goerdt et al. 2010). An alternative quantity for the LAB selection may be Lyα luminosity. However, the Lyα luminosity could be dominated by a bright central core, such as starbursts in the central galaxy and AGNs.

Table 1. Summary of narrow-band observations.

Field	RA (J2000)	Dec. (J2000)	Date (mm/yyyy)	Exposure (h)	Area (arcmin^2)	FWHM (arcsec)	Depth (cgs)[a]	Depth (ABmag)[b]
SXDS-C	02:18:00.0	−05:00:00	08, 09, 10/2005	5.2	682	1.0	0.81	26.3
SXDS-N	02:18:00.0	−04:35:00	10/2005	4.8	740	1.0	0.94	26.2
SXDS-S	02:18:00.0	−05:25:00	08, 10/2005	4.8	737	1.0	0.82	26.3
GOODS-N	12:37:23.6	+62:11:31	04/2005	10.0	869	1.1	0.69	26.6
SDF	13:24:39.0	+27:29:26	04/2004, 04/2005	7.2	805	1.0	0.67	26.5
SSA22-Sb1	22:17:34.0	+00:17:01	09/2002	7.2	633	1.0	0.92	26.3
SSA22-Sb2	22:16:36.7	+00:36:52	08/2004	5.5	487	1.0	0.96	26.3
SSA22-Sb3	22:18:36.3	+00:36:52	08, 09/2005	5.5	537	1.0	0.89	26.3
SSA22-Sb4	22:19:40.0	+00:17:00	08, 09, 10/2005	5.5	529	1.1	1.15	25.9
SSA22-Sb5	22:15:28.0	+00:17:00	09/2005	5.5	565	1.0	1.06	26.1
SSA22-Sb6	22:14:30.7	+00:33:52	10/2005	5.5	572	1.0	0.92	26.3
SSA22-Sb7	22:17:42.7	+00:56:52	09, 10/2005	5.5	480	1.0	1.02	26.2

[a]The 1σ surface brightness limit (10^{-18} erg s^{-1} cm^{-2} arcsec^{-2}).
[b]The 5σ limiting magnitude calculated with 2-arcsec-diameter aperture photometry.

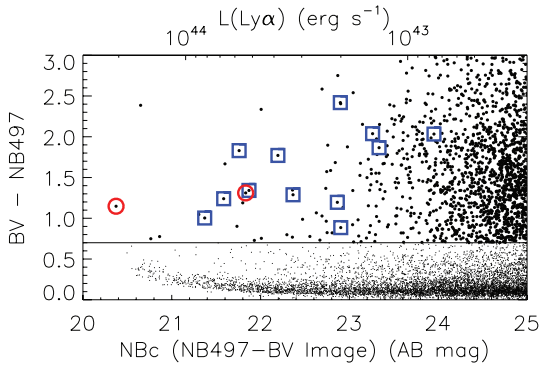

Figure 1. Colour–magnitude plot of $BV - NB497$ versus NB_c for NB_c-detected sources (black dots). The solid line represents the colour criterion ($BV - NB497 = 0.7$) used for narrow-band excess objects (larger dots). The blue squares and red circles indicate giant (major-axis diameters ≥ 100 kpc) LAB candidates without QSOs and with QSOs, respectively. All magnitudes and colours are measured with isophotal apertures.

Six out of the 14 LABs have been spectroscopically confirmed by previous surveys (Steidel et al. 2000; Barger et al. 2002; Matsuda et al. 2005, 2006; Shen et al. 2007). For two new LABs, we carried out spectroscopic follow-up observations with Magellan/IMACS in 2009 June and identified Lyα emission from these LABs (see Ono et al., in preparation for more details).

The properties of the 14 giant LABs are listed in Table 2. We rename the LABs in the new sample since initial surveys. SSA22-Sb1-LAB16 was named as LAB18 in Matsuda et al. (2004). Note that SSA22-Sb1-LAB1 discovered by Steidel et al. (2000) is still the largest one in this sample. SSA22-Sb3-LAB1 and GOODS-N-LAB1 are associated with quasi-stellar objects (QSOs) (Barger et al. 2002; Shen et al. 2007). We apply the 'QSO' label only to optically bright known QSOs, but some of the other LABs have potential signs of obscured AGNs. All the five LABs from the initial surveys (Steidel et al. 2000; Matsuda et al. 2004) were detected at X-ray, 8-μm and/or submillimetre (submm) wavelength follow-up observations (Chapman et al. 2001; Basu-Zych & Scharf 2004; Geach et al. 2005, 2009; Webb et al. 2009). Thus, although there are only two LABs apparently associated with QSOs, the AGN fraction of the 14 LABs may be higher when accounting for more obscured AGNs.

The thumbnail images (40×40 arcsec^2) of the 14 giant LABs are displayed in Fig. 2. The LABs show a wide variety of Lyα morphologies. While some LABs appear to have circular shapes, some have filamentary (or elongated) shapes. We quantify the Lyα morphology by defining 'filamentarity',

$$F \equiv 1 - \{(\text{isophotal area})/[\pi \times (a/2)^2]\},$$

where a is the major-axis diameter. For example, a circle has $F = 0$ and an extremely thin filament has $F = 1$. The filamentarities of the LABs range from $F \sim 0.4$ to 0.8. We estimate the uncertainties of the Lyα properties by putting the thumbnail NB_c images of each LAB at 100 random positions on the original NB_c images and measuring the deviations.

Fig. 3 shows the spatial distributions of the 14 giant LABs and smoothed density maps of ∼2000 Lyα emitters (LAEs) selected by Yamada et al. (in preparation) with the same data. Since some bright Lyα knots in the giant LABs are also detected as single or multiple LAEs, we exclude such LAEs from the LAE sample in this analysis. We make the density maps by smoothing the LAE spatial distributions with a Gaussian kernel of $\sigma = 1.2$ arcmin or FWHM = 5.3 comoving Mpc. The smoothing kernel size is chosen to match the median distance between the nearest neighbours in the LAE samples in the blank fields (SXDS, GOODS-N and SDF). The contours represent LAE overdensities, $\delta_{\rm LAE} \equiv (n - \bar{n})/\bar{n} = 0$, 1, 2, 3, 4, 5 and 6, where $\bar{n}$ is the mean LAE number density in the blank fields.

In Fig. 4, we plot the filamentarities of the 14 LABs as a function of the LAE overdensities. The filamentarity shows a weak anticorrelation with the LAE overdensity. While more filamentary LABs reside in average density environments, more circular LABs reside in both average density and overdense environments. Spearman's rank correlation coefficient is $r_s = -0.56$. We can rule out random distributions with 96 per cent confidence. We have confirmed that the results do not change significantly, if we use isophotal area for the LAB selection, suggesting that the correlation is not due to the selection method.

Table 2. Properties of the 14 giant LAB candidates.

ID	RA (J2000)	Dec. (J2000)	a[a] (kpc)	Area (arcsec^2)	$L_{\rm Ly\alpha}$ (10^{43} erg s^{-1})	F[b]	$\delta_{\rm LAE}$	$z_{\rm spec}$	Note
SSA22-Sb1-LAB1	22:17:25.95	+00:12:37.7	175	181 ± 14	8.1 ± 0.6	0.56	2.7	3.099[c]	8 μm[i]/submm[j]
SSA22-Sb6-LAB1	22:13:48.30	+00:31:32.8	166	116 ± 9	5.8 ± 0.4	0.69	0.6	3.094[d]	–
SSA22-Sb1-LAB2	22:17:38.99	+00:13:27.8	157	137 ± 8	6.8 ± 0.3	0.59	3.7	3.091[c]	X-ray[k]/8 μm[i]
SSA22-Sb5-LAB1	22:15:33.56	+00:25:16.9	147	59 ± 7	3.8 ± 0.4	0.80	−0.5	–	–
SSA22-Sb3-LAB1	22:17:59.45	+00:30:55.7	126	102 ± 8	20.4 ± 0.3	0.52	1.2	3.099[e]	QSO[e]/radio[l]
GOODS-N-LAB1	12:35:57.54	+62:10:24.9	124	47 ± 7	5.4 ± 0.5	0.77	0.9	3.075[f]	QSO[f]/X-ray[m]
SSA22-Sb2-LAB1	22:16:58.37	+00:34:32.0	121	60 ± 15	2.0 ± 0.6	0.70	1.2	–	–
SSA22-Sb2-LAB2	22:16:56.40	+00:27:53.3	115	48 ± 11	1.4 ± 0.2	0.73	−0.1	–	–
SSA22-Sb1-LAB5	22:17:11.66	+00:16:44.4	110	43 ± 11	1.3 ± 0.3	0.74	1.0	–	8 μm[i]/submm[n]
SSA22-Sb5-LAB2	22:15:30.27	+00:27:43.6	107	53 ± 7	2.1 ± 0.3	0.66	−0.1	–	–
SSA22-Sb6-LAB4	22:14:09.58	+00:40:54.6	107	32 ± 4	2.0 ± 0.2	0.79	−0.1	3.116[d]	–
SSA22-Sb1-LAB3	22:17:59.14	+00:15:28.7	103	75 ± 9	5.2 ± 0.2	0.48	1.7	3.096[g]	X-ray[l]
SXDS-N-LAB1	02:18:21.31	−04:42:33.1	101	68 ± 5	3.3 ± 0.2	0.51	−0.4	–	–
SSA22-Sb1-LAB16	22:17:29.01	+00:07:50.2	101	28 ± 8	0.8 ± 0.2	0.80	−0.2	3.104[h]	X-ray[l]/8 μm[i]/submm[n]

[a]Major-axis diameter; [b]filamentarity ($F = 0$ for a circle, $F = 1$ for a filament, see text for more detail); [c]Steidel et al. (2003); [d]this work; [e]Shen et al. (2007); [f]Barger et al. (2002); [g]Matsuda et al. (2005); [h]Matsuda et al. (2006); [i]Webb et al. (2009); [j]Chapman et al. (2001); [k]Basu-Zych & Scharf (2004); [l]Condon et al. (1998); [m]Alexander et al. (2003); [n]Geach et al. (2005); [l]Geach et al. (2009).

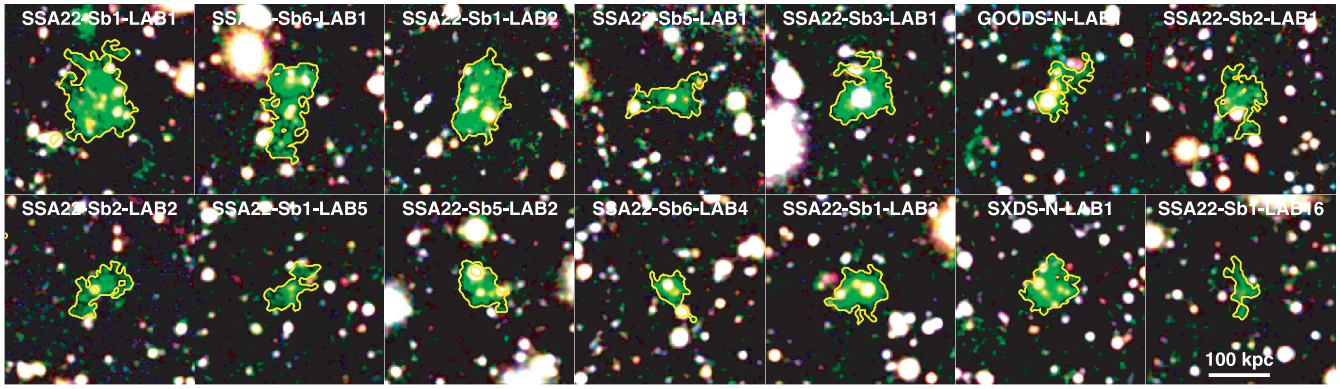

Figure 2. Pseudo-colour images (*B* for blue, *NB*497 for green, *V* for red) of the 14 giant LABs. The size of the images is 40 × 40 arcsec^2 (∼300 × 300 kpc^2). The yellow contours indicate isophotal apertures with a threshold of 1.4×10^{-18} erg s^{-1} cm^{-2} arcsec^{-2}. The white horizontal bar in the lower right-hand image represents the angular scale of 100 kpc (physical scale) at $z = 3.1$.

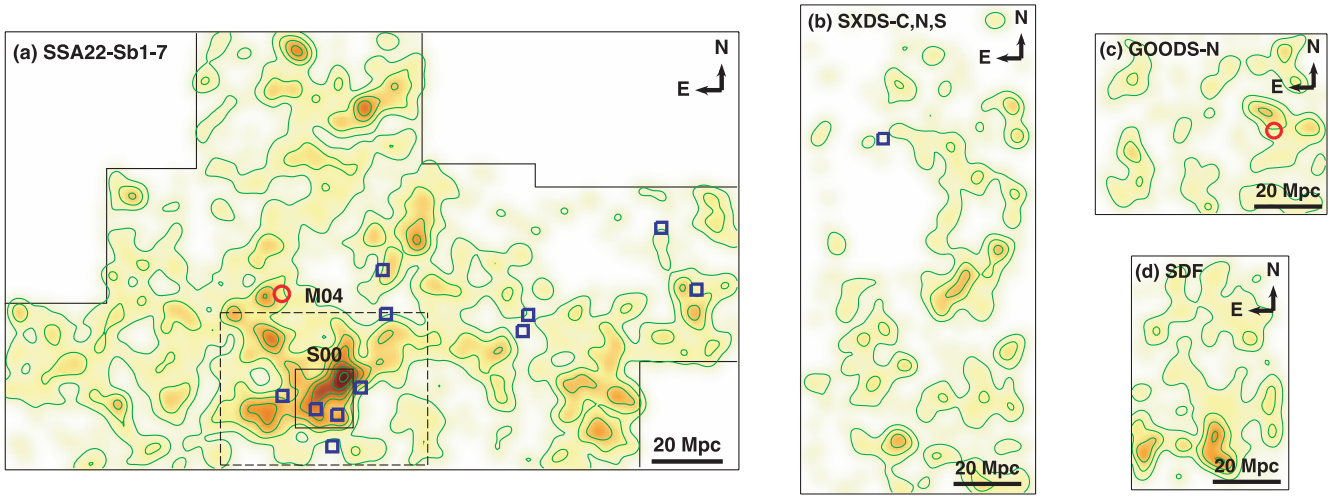

Figure 3. Sky distribution of the 14 giant LABs and smoothed density maps of ∼2000 compact LAEs at $z \sim 3.09$. In the left-hand panel (a), the small black box indicates the SSA22a field by Steidel et al. (2000, S00) and the dashed box indicates the SSA22-Sb1 field by Matsuda et al. (2004, M04). The thick bars show the angular scale of 20 comoving Mpc at $z = 3.1$. The blue squares and red circles indicate the giant LABs without QSOs and with QSOs, respectively. The contours represent LAE overdensity, $\delta_{\rm LAE} \equiv (n - \bar{n})/\bar{n}$ =0, 1, 2, 3, 4, 5 and 6.

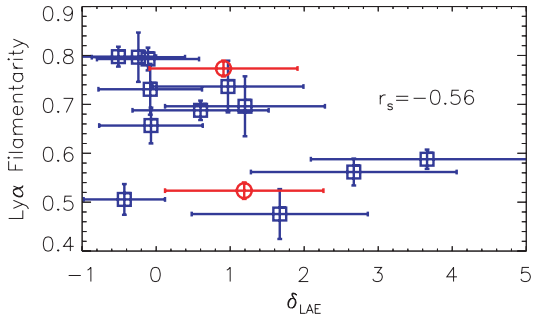

Figure 4. Filamentarity of the 14 giant LABs as a function of the overdensity of LAEs. The blue squares and red circles indicate giant LABs without QSOs and with QSOs, respectively. The error bars show 1σ uncertainties. The filamentarity of the LABs shows a weak anticorrelation with the overdensity of LAEs.

4 DISCUSSION AND CONCLUSIONS

Based on deep, wide-field Lyα imaging, we construct a sample of 14 giant LAB candidates at $z = 3.1$ from a volume of 1.6×10^6 comoving Mpc^3. This is the largest sample of giant LABs and triples the number of known LABs over 100 kpc. Our giant LAB sample shows a wide variety of Lyα morphologies and resides not only in overdense environments, as derived from LAEs, but also in low-dense environments. We find a possible hint for the 'morphology–density' relation of the LABs: the Lyα filamentarity seems to differ as a function of the local density environments.

How can we interpret this possible morphology–density relation of the LABs? The Lyα morphology may relate to the formation mechanisms of LABs. According to recent numerical simulations, more filamentary LABs may be good candidates for cold gas accretion from the surrounding IGM (Faucher-Giguere et al. 2010; Goerdt et al. 2010). Although direct evidence for such gas inflows is not found around star-forming galaxies at $z \sim 2$ (Steidel et al. 2010), recent studies of the metallicity of star-forming galaxies from low to high redshifts indicate that gas inflows may still be dominant in the field environment at $z \gtrsim 3$ (Mannucci et al. 2010). More circular LABs may relate to large-scale gas outflows, which are driven by intense starbursts and/or AGN activities (Mori & Umemura 2006). At high redshift, star-formation and AGN activities in overdense environments are known to be several times higher than those in

the field environments (e.g. Smail et al. 2003). Future spectroscopic and multiwavelength follow-up observations would enable us to investigate the gas dynamics and the variations in the star-formation and AGN activities in giant LABs as a function of the environments, and to test the interpretations.

ACKNOWLEDGMENTS

We thank an anonymous referee for helpful comments, which significantly improved the clarity of this paper. We thank Ian Smail for help and useful discussions. YM acknowledges support from STFC. This research was supported in part by the Grant-in-Aid 20540224 for Scientific Research of the Ministry of Education, Science, Culture, and Sports in Japan.

REFERENCES

Alexander D. M. et al., 2003, AJ, 126, 539
Barger A. J. et al., 2002, AJ, 124, 1839
Basu-Zych A., Scharf C., 2004, ApJ, 615, L85
Bertin E., Arnouts S., 1996, A&A, 117, 393
Capak P. et al., 2004, AJ, 127, 180
Chapman S. C. et al., 2001, ApJ, 548, L17
Condon J. J. et al., 1998, AJ, 115, 1693
Cutri R. M. et al., 2003, The IRSA 2MASS All-Sky Point Source Catalog, NASA/IPAC Infrared Science Archive, http://irsa.ipac.caltech.edu/applications/Gator/
Dey A. et al., 2005, ApJ, 629, 654
Dijkstra M., Loeb A., 2009, MNRAS, 400, 1109
Faucher-Giguere C. et al., 2010, ApJ, in press (arXiv:1005.3041)
Francis P. J. et al., 1996, ApJ, 457, 490
Furlanetto S. R., Schaye J., Springel V., Hernquist L., 2005, ApJ, 622, 7
Furusawa H. et al., 2008, ApJS, 176, 1
Geach J. E. et al., 2005, MNRAS, 363, 1398
Geach J. E. et al., 2009, ApJ, 700, 1
Goerdt T., Dekel A., Sternberg A., Ceverino D., Teyssier R., Primack J. R., 2010, MNRAS, 407, 613
Greve T. R. et al., 2007, MNRAS, 382, 48
Haiman Z., Spaans M., Quataert E., 2000, ApJ, 537, L5
Hayashino T. et al., 2004, AJ, 128, 2073
Iye M. et al., 2004, PASJ, 56, 381
Kashikawa N. et al., 2004, PASJ, 56, 1011
Keel W. C., Cohen S. H., Windhorst R. A., Waddington I., 1999, AJ, 118, 2547
Landolt A. U., 1992, AJ, 104, 340
Mannucci F., Cresci G., Maiolino R., Marconi A., Gnerucci A., 2010, MNRAS, 408, 2115
Matsuda Y. et al., 2004, AJ, 128, 569
Matsuda Y. et al., 2005, ApJ, 634, L125
Matsuda Y. et al., 2006, ApJ, 640, L123
Matsuda Y. et al., 2009, MNRAS, 400, L66
Miyazaki S. et al., 2002, PASJ, 54, 833
Mori M., Umemura M., 2006, Nat, 440, 644
Nilsson K. K. et al., 2006, A&A, 452, L23
Oke J. B., 1990, AJ, 99, 1621
Ouchi M. et al., 2003, ApJ, 582, 60
Ouchi M. et al., 2009, ApJ, 696, 1164
Palunas P. et al., 2004, ApJ, 602, 545
Prescott M. K. M., Kashikawa N., Dey A., Matsuda Y., 2008, ApJ, 678, L77
Prescott M. K. M., Dey A., Jannuzi B. T., 2009, ApJ, 702, 554
Saito T., Shimasaku K., Okamura S., Ouchi M., Akiyama M., Yoshida M., 2006, ApJ, 648, 54
Saito T., Shimasaku K., Okamura S., Ouchi M., Akiyama M., Yoshida M., Ueda Y., 2008, ApJ, 675, 1076
Scarlata C. et al., 2009, ApJ, 706, 1241
Schlegel D. J., Finkbeiner D. P., Davis M., 1998, ApJ, 500, 525
Shen Y. et al., 2007, AJ, 133, 2222
Shimizu I., Umemura M., 2010, MNRAS, 406, 913
Smail I. et al., 2003, ApJ, 599, 86
Smith D. J. B., Jarvis M. J., 2007, MNRAS, 378, L49
Steidel C. C. et al., 2000, ApJ, 532, 170
Steidel C. C. et al., 2003, ApJ, 592, 728
Steidel C. C., Erb D. K., Shapley A. E., Pettini M., Reddy N., Bogosavljević M., Rudie G. C., Rakic O., 2010, ApJ, 717, 289
Taniguchi Y., Shioya Y., 2000, ApJ, 532, L13
Yagi M. et al., 2002, AJ, 123, 66
Yang Y. et al., 2009, ApJ, 693, 1579
Yang Y., Zabludoff A., Eisenstein D., Davé R., 2010, ApJ, 719, 1654
Webb T. M. A. et al., 2009, ApJ, 692, 1561

This paper has been typeset from a TEX/LATEX file prepared by the author.